LASER INTERFEROMETER GRAVITATIONAL WAVE OBSERVATORY
- LIGO -
CALIFORNIA INSTITUTE OF TECHNOLOGY
MASSACHUSETTS INSTITUTE OF TECHNOLOGY

Technical Note **LIGO-T1700336–v1** 2017/09/08

Squeezing Quantum Noise with Waveguides
Project Report for SURF 2017

Dhruva Ganapathy

California Institute of Technology
LIGO Project, MS 18-34
Pasadena, CA 91125
Phone (626) 395-2129
Fax (626) 304-9834
E-mail: info@ligo.caltech.edu

Massachusetts Institute of Technology
LIGO Project, Room NW22-295
Cambridge, MA 02139
Phone (617) 253-4824
Fax (617) 253-7014
E-mail: info@ligo.mit.edu

LIGO Hanford Observatory
Route 10, Mile Marker 2
Richland, WA 99352
Phone (509) 372-8106
Fax (509) 372-8137
E-mail: info@ligo.caltech.edu

LIGO Livingston Observatory
19100 LIGO Lane
Livingston, LA 70754
Phone (225) 686-3100
Fax (225) 686-7189
E-mail: info@ligo.caltech.edu

http://www.ligo.caltech.edu/

1 Introduction

1.1 LIGO

The LIGO gravitational wave detectors are specialized versions of a Michelson interferometer with 4 km long arms with Fabry Perot cavities. Its peak design sensitivity is 3.5×10^{-24} in the 100 Hz band[1]. The Advanced LIGO (aLIGO) detectors came online in September 2015, after a major upgrade targeting a factor of 10 sensitivity improvement over initial detectors. The two test masses are placed 4 km apart and form an optical resonator with a gain of 300. The suspension system provides high isolation above the resonance frequencies which range from 0.4 to 13 Hz.

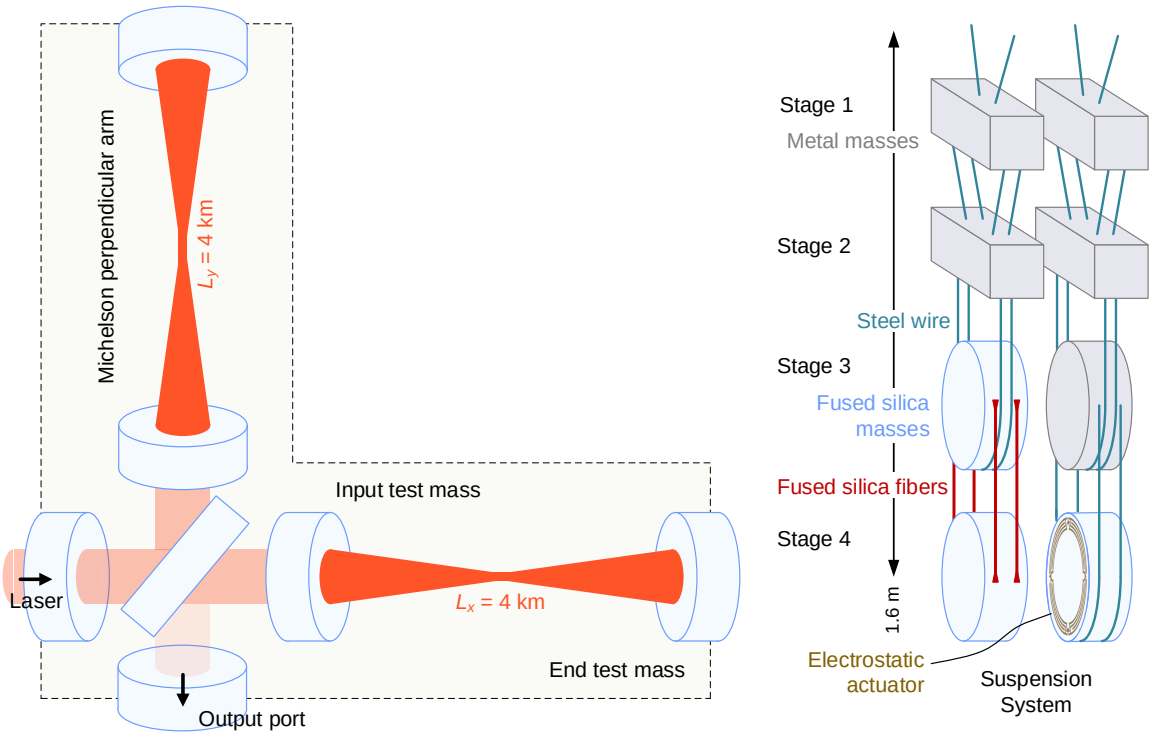

Figure 1: aLIGO

1.2 Quantum Noise in aLIGO

When it reaches aLIGO design sensitivity it will be quantum noise limited over much of the detection band[2]. The quantum noise in LIGO, which is due to the vacuum fluctuations entering the dark port of the interferometer, is the sum of Quantum Shot Noise, which is due to the difference in arrival timings of photons at the detector and Radiation Pressure noise which is due the the mirror movement caused by amplitude fluctuations in light which result in fluctuating radiation pressure.

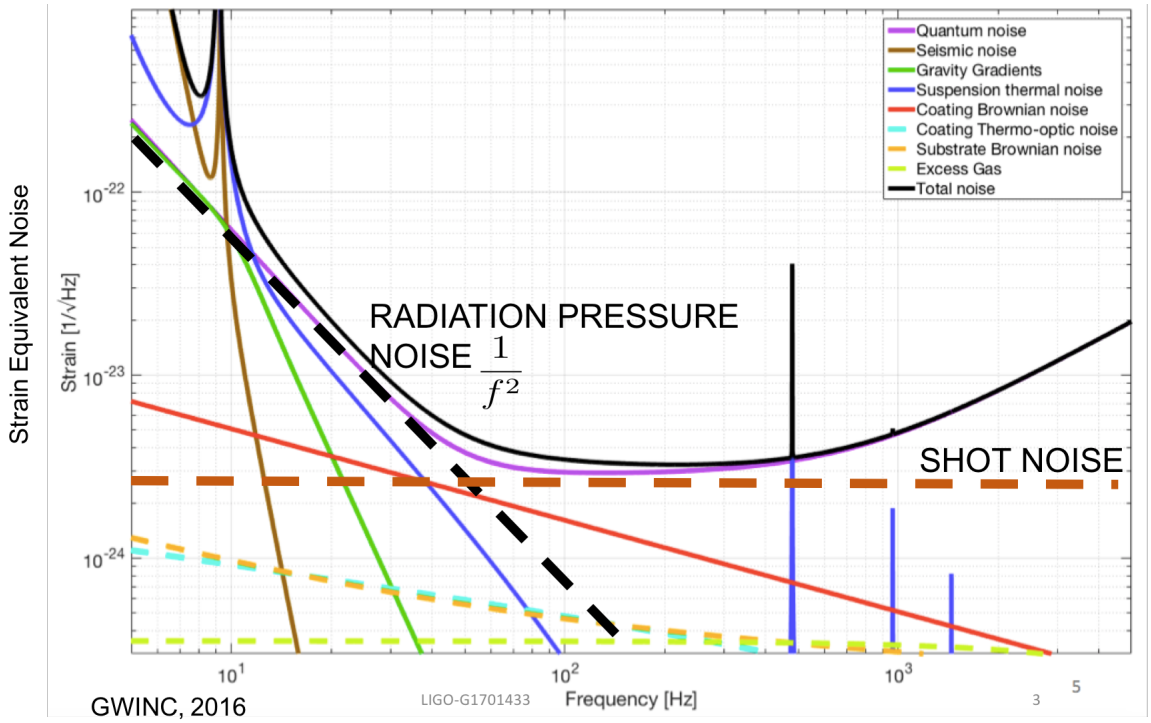

Figure 2: aLIGO Sensitivity Curve

2 Background

2.1 Squeezed Light

In an upgrade to aLIGO [3], work is underway to install a parametric oscillator squeezed vacuum light source to reduce the quantum shot noise which limits the sensitivity of gravitational wave detector. This noise arises due to vacuum fluctuations which occur due to Heisenbergs uncertainty principle which states that $\Delta X \Delta Y > 1$ where X and Y are uncertainty in the quadratures associated with the photon field and are given by the expressions :

$$\hat{X} = (\hat{a} + \hat{a}^\dagger)$$
$$\hat{Y} = -i(\hat{a} - \hat{a}^\dagger)$$

Where a and $a^\dagger$ are bosonic annihilation and creation operators respectively. Coherent states are minimum uncertainty states where $\Delta X = \Delta Y = 1$. Vacuum states are a special case of the coherent state and are the ground state and lowest energy state of the photon field. These uncertainties give rise to vacuum fluctuations which enter the open anti-symmetric port of the gravitational wave detector generating uncertainty in the readout of electromagnetic fields on detection. The variance in the electric field can be given in terms of the variance in quadratures.

$$\Delta\hat{E} \propto \Delta X(sin^2(\omega t)) + \Delta Y(cos^2(\omega t))$$

The noise arising from these uncertainties can be understood by Figure 3. White noise in the time domain translates to equal variance in quadratures.

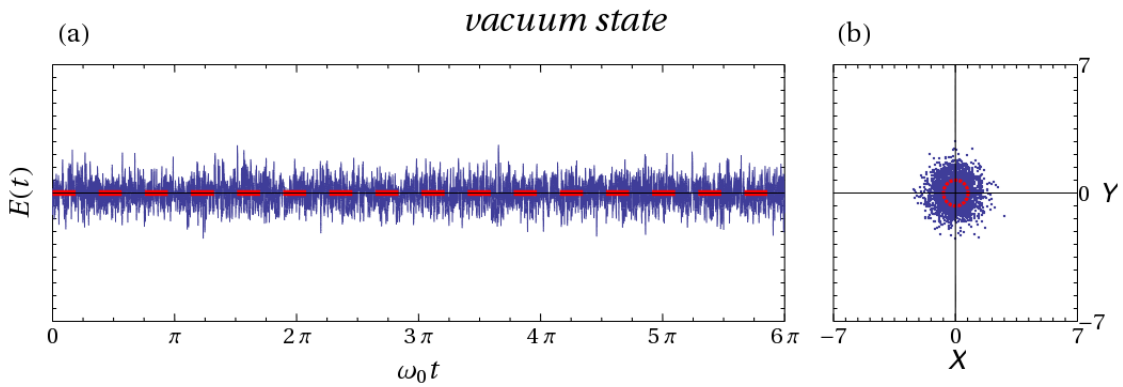

Figure 3: Electric Field in Coherent Vacuum

Squeezed states are also minimum uncertainty states. Here, the noise in one quadrature is greater than that in the other. In the time domain, this translates to increase in phase(intensity) noise and decrease in the other. Replacing the vacuum fluctuations with squeezed states in GW interferometers can reduce the quantum noise measured by the detector.

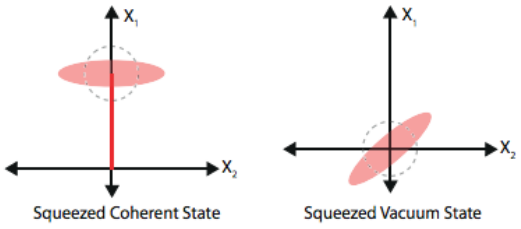

Figure 4: Quadrature Diagrams for Squeezed Light. The width of the ellipse in a given direction gives the uncertainty in the quadrature in that direction

Squeezing has already been implemented twice in working GW detectors [4],[5] and once in the Caltech 40m prototype[7] and, is a proven technology for enhancing signal to shot noise sensitive by 3.5 dB and 2.1 dB for the GEO600 and Enhanced LIGO detectors respectively. Squeezing injection is planned as a permanent feature in the next round of intermediate upgrades. More details about squeezed light can be found in [6].

2.1.1 Mode Matching and Beam Propagation

One part of this project would involve modelling mode-matching between the wave-guide and the optical cavity of the resonator. For the optical waveguide, we will be considering a rectangular core waveguide with a step index.

To find the mode shapes of this waveguide, we can assume a separable solution of the scalar wave equation in rectangular coordinates.

$$\frac{\partial^2\psi}{\partial x^2} + \frac{\partial^2\psi}{\partial y^2} + [k_o^2 n^2(x,y) - \beta^2] = 0 \tag{1}$$

where β is the propagation constant and k_o is the free space wave number.

The solution obtained for this equation is given by

$$\psi = \begin{cases} A\cos\mu_1\xi\cos\mu_2\eta & \text{if}|\xi| \le 1, |\eta| \le 1 \\ \dfrac{A\cos\mu_2}{\exp[-(V_2^2-\mu_2^2)]^{\frac{1}{2}}}\cos\mu_1\xi\exp[-(V_2^2-\mu_2^2)\eta]^{\frac{1}{2}} & \text{if } |\xi| \ge 1, |\eta| \le 1 \\ \dfrac{A\cos\mu_1}{\exp[-(V_1^2-\mu_1^2)]^{\frac{1}{2}}}\cos\mu_2\eta\exp[-(V_1^2-\mu_1^2)\xi]^{\frac{1}{2}} & \text{if } |\xi| \le 1, |\eta| \ge 1 \\ \dfrac{\exp[-(V_2^2-\mu_2^2)\eta]^{\frac{1}{2}}\exp[-(V_1^2-\mu_1^2)\xi]^{\frac{1}{2}}}{\exp[-(V_1^2-\mu_1^2)]^{\frac{1}{2}}\exp[-(V_2^2-\mu_2^2)]^{\frac{1}{2}}} & \text{if } |\xi| \ge 1, |\eta| \ge 1 \end{cases} \tag{2}$$

where

$$\xi = (2x/a), \quad \eta = (2y/b), \quad V_1 = k_o\frac{a}{2}(n_1^2 - n_2^2)^{\frac{1}{2}}, \quad V_2 = k_o\frac{b}{2}(n_1^2 - n_2^2)^{\frac{1}{2}}$$

$$\mu_1 = \frac{a}{2}(k_o^2 n_1^2 - \beta^2)^{\frac{1}{2}}, \quad \mu_2 = \frac{b}{2}(k_o^2 n_1^2 - \beta^2)^{\frac{1}{2}}$$

A detailed solution of this equation is described in [8]. The effect of imperfections in the step index can be modelled by methods such as perturbation and scalar variational methods.

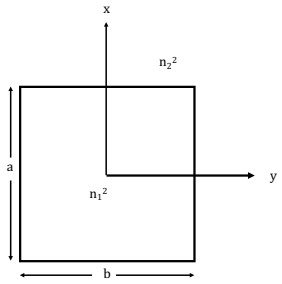

Figure 5: Rectangular Core Waveguide. n_1^2 and n_2^2 are core and cladding refractive indices

The normal modes supported by the optical cavity, or any complex paraxial optical system, are higher order Gaussian or Hermite-Gaussian modes. These modes are given by

$$\tilde{u}_n = \tilde{\alpha}_n\tilde{v}^n H_n(\frac{\sqrt{2}x}{\tilde{v}})\exp(-\frac{r^2}{w(z)^2})\exp(-i\frac{kr^2}{2R(z)})\exp(-i(kz - \psi(z)))$$

where H_n is the n^{th} order Hermite polynomial, and $\psi(z)$ is the Gouy Phase of the beam

2.2 Beam Propagation

2.2.1 ABCD Propagation

When a Gaussian beam propagates in free space, it remains Gaussian, while its spot size and radius of curvature vary according to the wave equation. Now the beam at a point can be characterised by the following quantity.

$$q = z + iz_r$$

where z_r is the Rayleigh range of the beam, and z is the distance of the point from the waist.

The inverse of q contains a information about the spot size and radius of curvature of the beam. Substituting $w(z)$ and $R(z)$, we get

$$\frac{1}{q} = \frac{1}{R(z)} - \frac{i\lambda}{\pi w^2(z)}$$

If we specify the initial value of q, then we can use the ABCD propagation matrices for determining the final value of q[9].

$$q_2 = \frac{Aq_1 + B}{Cq_1 + D}$$

The matrices that we use in this project are -

$$\mathbf{M}_{prop} = \begin{pmatrix} 1 & d \\ 0 & 1 \end{pmatrix}$$

for free space propagation through distance d and

$$\mathbf{M}_{prop} = \begin{pmatrix} 1 & 0 \\ -\frac{1}{f} & 1 \end{pmatrix}$$

for propagation through lens with focal length f.

2.2.2 FFT Propagation

While ABCD propagation is a convinient method and can be used as a reference for other propagation methods, it is only applicable to the mode shapes that satisfy the paraxial approximation, i.e. Gaussian beams. The mode outside the waveguide will not be a Gaussian and we will need other methods to find its mode shape after propagation in free space. One such method that we have implemented is FFT propagation of the beam[10].

According to the Huygens integral,

$$E(x, y, z) = \frac{i}{\Delta z \lambda} \iint E_0(x, y, z_0) K(x - u, y - v, \Delta z) du dv$$

which can be seen as a convolution of the source field E_0 at z_0 and the paraxial diffraction kernel.

In the fourier space, this is just the product of the Fourier Transform of the field and the FT of the diffraction kernel which is given by

$$\tilde{K}(p, q, \Delta z) = \exp\left(-i\frac{\Delta z(p^2 + q^2)}{2k}\right)$$

.

The final mode can be found out by taking an inverse fourier transform of the product. In our code we have used the fft2, and ifft2 functions of MATLAB to implement this routine.

2.2.3 Detecting Squeezed States

Balanced homodyne is an interference setup that is used for quadrature measurements. The field that is to be measured is overlapped with a local oscillator on a symmetric beam splitter, whose outputs impinge of two photodiodes, whose photocurrents are electronically subtracted. The phase of the local oscillator beam is controlled via a piezzo-electric transducer. The subtracted photocurrent is analysed using time domain and frequency domain approaches as described in [6].

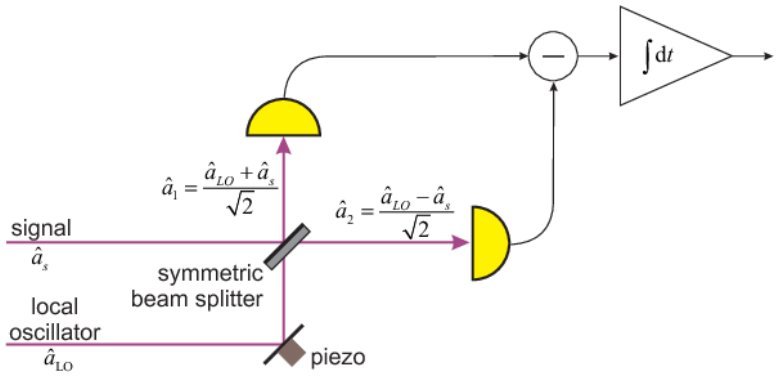

Figure 6: Balanced Homodyning Scheme

In order to properly detect squeezed states, we also need to take into account the noise that affects the homodyning process. The source of this noise includes electronic noise such as flicker in resistors and dark noise of photodiode, and optical noise due to scattering loss, photodiode inhomogeneity and parasitic interferences. These sources and methods to reduce them have been described in [11].

3 Objective and Project Setup

In project, we designed a Waveguide squeezer setup for 1064nm light using a Rubidium infused PPKTP non linear waveguide. The project setup is shown in Figure 7. The Innolight

Diabolo laser is a source of 532 nm and 1064 nm photons for the experiment. It consists of a 1.5 W Nd:YAG NPRO laser (pumped with two banks of diode lasers) with most of this light tapped off to an SHG unit for conversion to 532 nm. The green 532nm photons undergo Spontaneous Parametric Down-Conversion in a compact non-linear waveguide. Single mode squeezing is obtained when the SPDC is degenerate, i.e, the produced photons are indistinguishable.

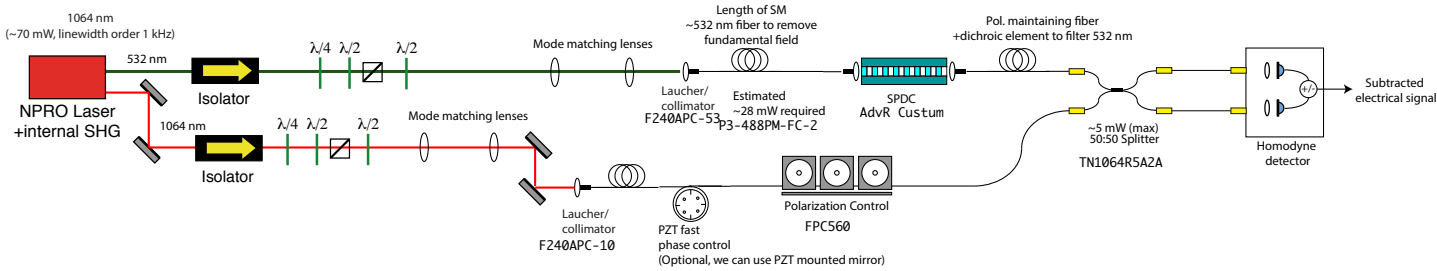

Figure 7: Initially Proposed Setup for Waveguide Experiment. The 1064nm beam is used as the local oscillator(adjustable phase and polarization) while the 532nm beam is used for squeezing(through SPDC in the non linear waveguide). The two beams are sent through a fibre beam-splitter for balanced homodyne detection.

3.1 Approach

The project can be divided into three major parts -

- Coupling of light from free space into fibres using mode matching lenses;
- Squeezing the fibre coupled light in the non-linear waveguide;
- Detecting the squeezed states of light using balanced homodyne detection;

4 Progress

4.1 Mode Matching Light into Fibres

Figure 8 describes the internal working of the Diabolo laser and shows the two different outputs. Figure 9 shows the mode matching setup.

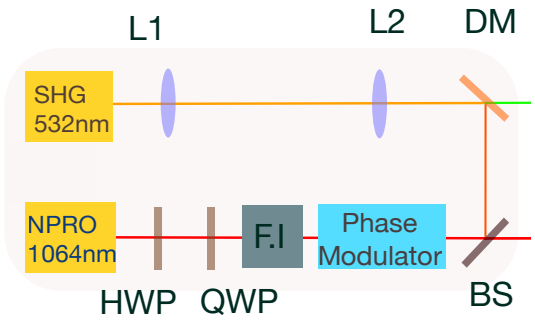

Figure 8: Innolight Diabolo. An NPRO(Non Planar Ring Oscillator) is used as the 1064nm laser source. A part of the 1064nm beam is up-converted by an SHG Cavity to produce the 532nm beam.

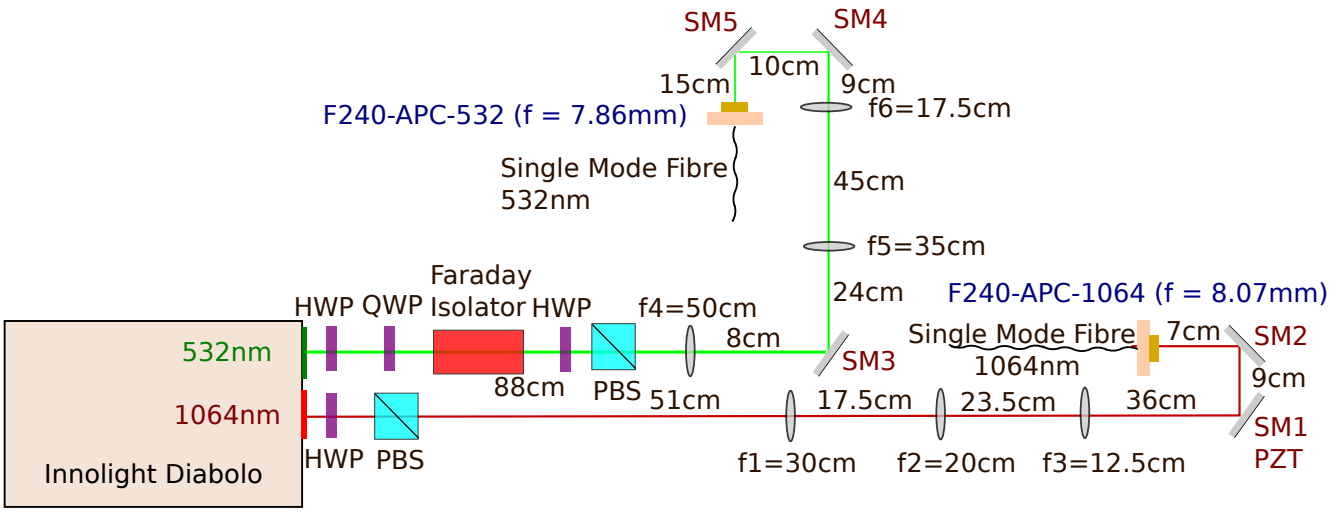

Figure 9: Mode Matching Setup. There are two beam paths (1064nm and 532nm) and the path lengths are indicated in the labels

In 8, L1 and L2 are mode matching lenses, DM is a dichroic mirror which reflects 1064nm and transmits 532nm, BS is a 50% beamsplitter, and F.I is a Faraday Isolator. In figure

9, F240-APC-1064 is the collimation package for transmitting the laser from free space into the 1064nm Single mode fibre and F240-APC-532 is the collimation package for the 532nm beam. SM1 is a PZT actuated mirror which will be used for the phase control of the local oscillator.

4.1.1 Beam Profiling

The following are the results of profiling the 1064nm and 532 nm beams from the Innolight Diabolo laser.

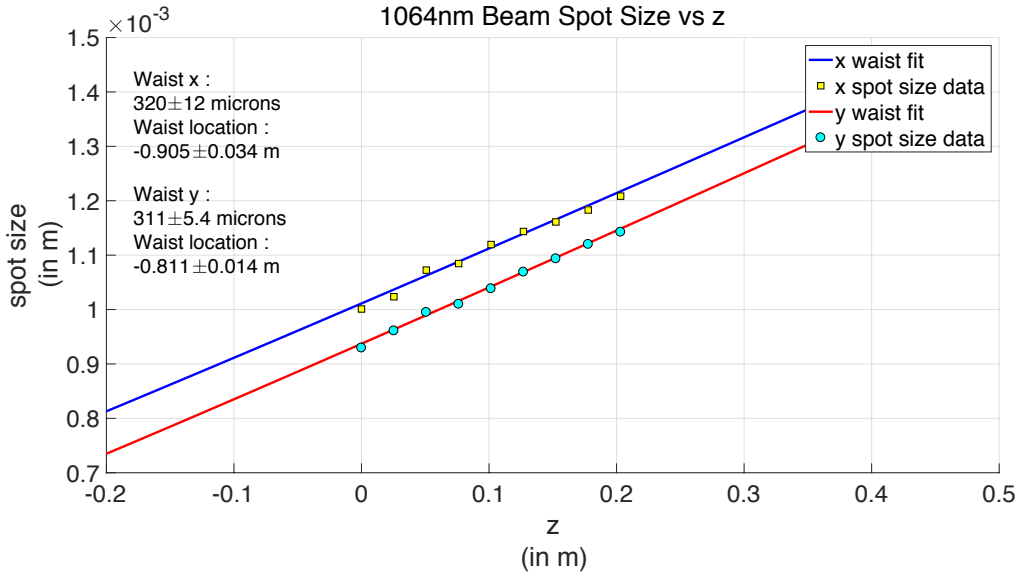

Figure 10: Beam Profiling the 1064nm laser

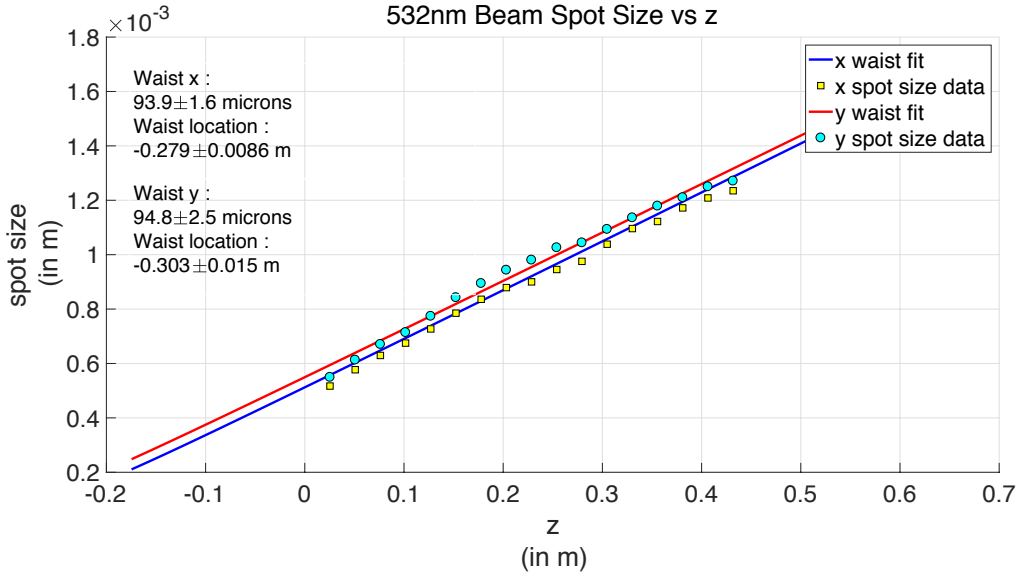

Figure 11: Beam Profiling the 532nm laser

4.1.2 Mode Matching of 1064nm Beam

The 1064nm beam is collimated in free space and then focused into a single mode fibre with the help of the collimation package F240-APC-1064. This package has a collimated beam size of 880 μm and a beam divergence of 0.04 degrees. In order to achieve efficient coupling, we needed to make sure that the beam waist of the beam that we are focusing into the fibre is close to the above size. Working at a 3 lens solution, we first added a lens (f=30cm) in the beam path at z = 105cm, and profiled the beam again to find a more accurate value for the beam waist size and location.

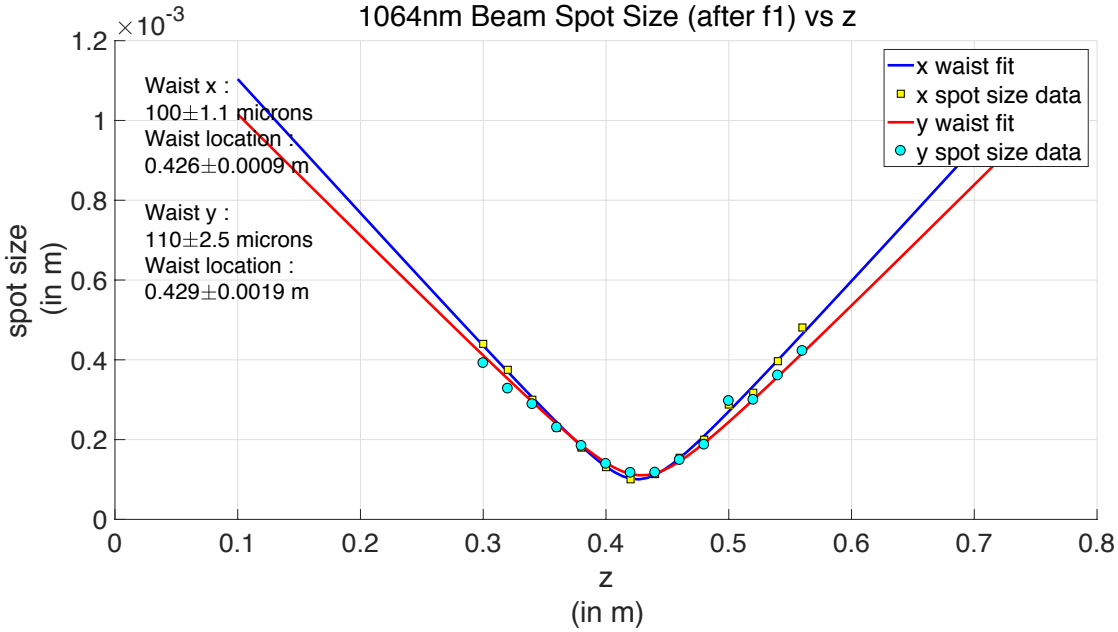

Figure 12: A 1064nm beam profile after the first lens. z=0 is the location of the lens

Trial and error gave us a modified value of the initial beam waist to be 275 μm and location as -80cm from the arbitrarily chosen z=0 point. Over here, for the sake of simplicity, we assume that the x and y waists of the beam are approximately equal as the amount of squeezing does not depend on the coupling efficiency at this interface and we just need significant power in the fibre.

Using these modified values, we calculated a mode-matching solution with 3 lenses using ABCD propagation.

The 3 lens solution Figure 13 is as follows :
f = 30cm at z = 105cm
f = 20cm at z = 122.5cm
f = 12.5cm at z = 146cm

The obtained beam waist of the collimated beam was 855.9 μm that is very close to the required 880 μm. Neglecting beam divergence of the collimator, we obtained the theoretical coupling efficiency to be 99.8%. The actual mode matching that is possible to achieve is lower than this because there are many factors to account for like defects in the lens, or

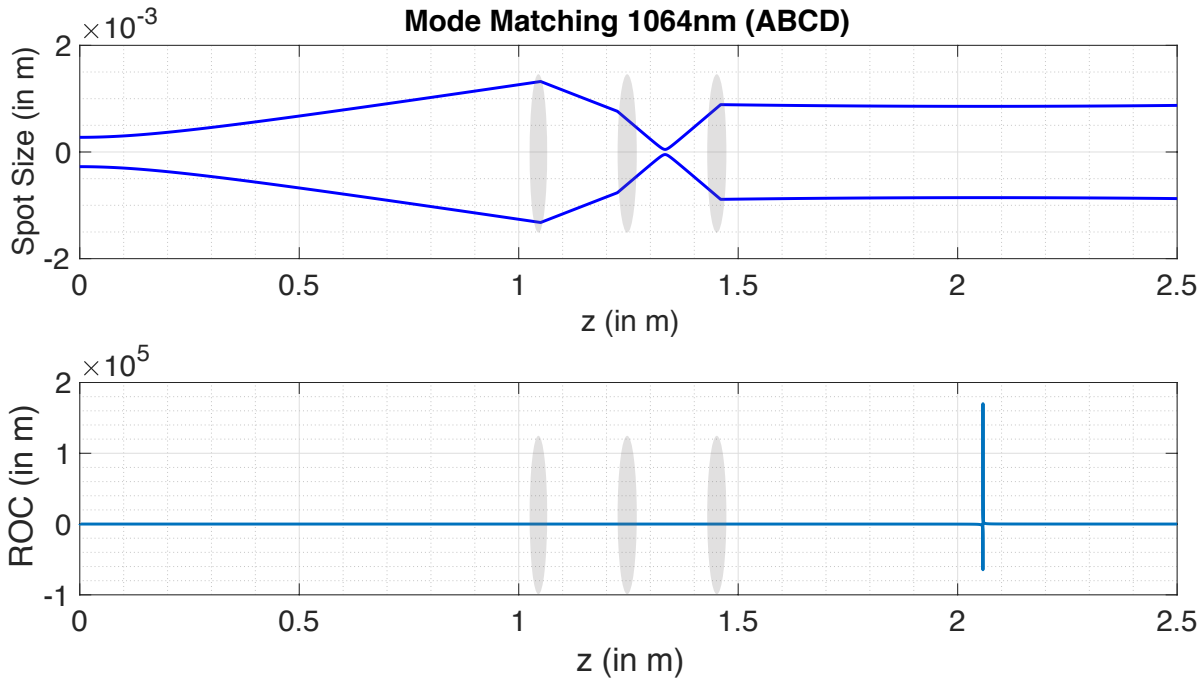

Figure 13: Mode Matching Solution for 1064nm (Waist at z=0)

astigmatism of the beam and the errors in lens locations.

In order to confirm this solution, we profiled the beam after placing the second lens (f=20cm) at z=122.5cm.

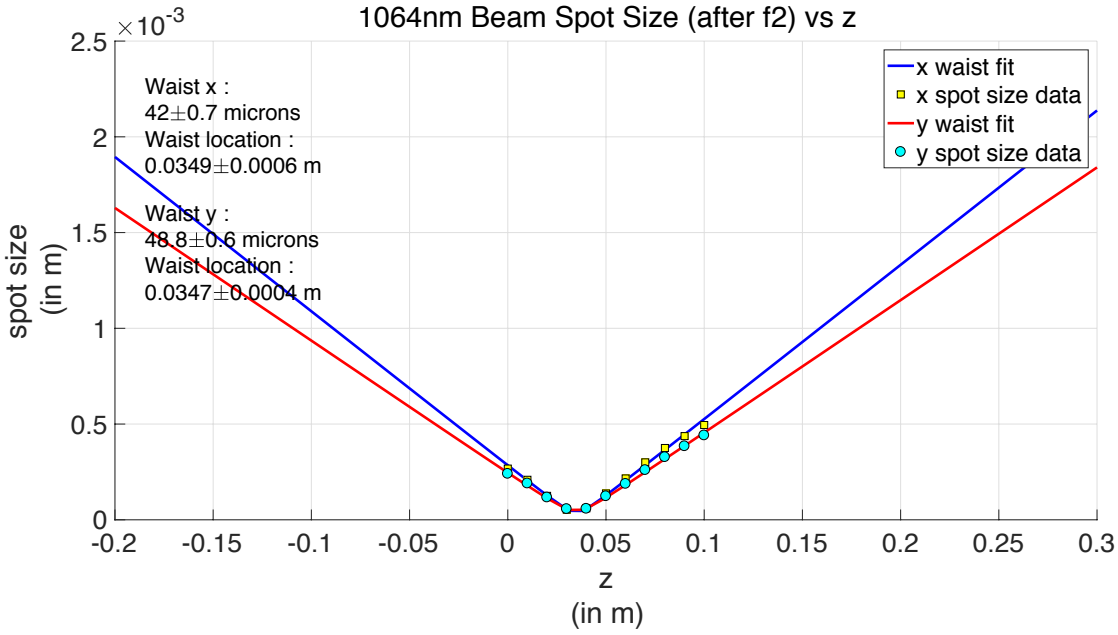

Figure 14: A 1064nm beam profile after the second lens. z=0 is the location of the lens

The size and location of the second waist corresponds to that obtained by the ABCD simulation of the solution.

Using the above configuration with some fine tuning, we managed to achieve around **75.4%** efficiency in coupling.

4.1.3 Mode Matching of 532nm Beam

Just like the 1064nm beam, we also need to mode match the 532nm beam into a fibre using F240APC-532 collimation package. The required beam spot size for this is 740 μm. The solution that we obtain using ABCD propagation is as follows -

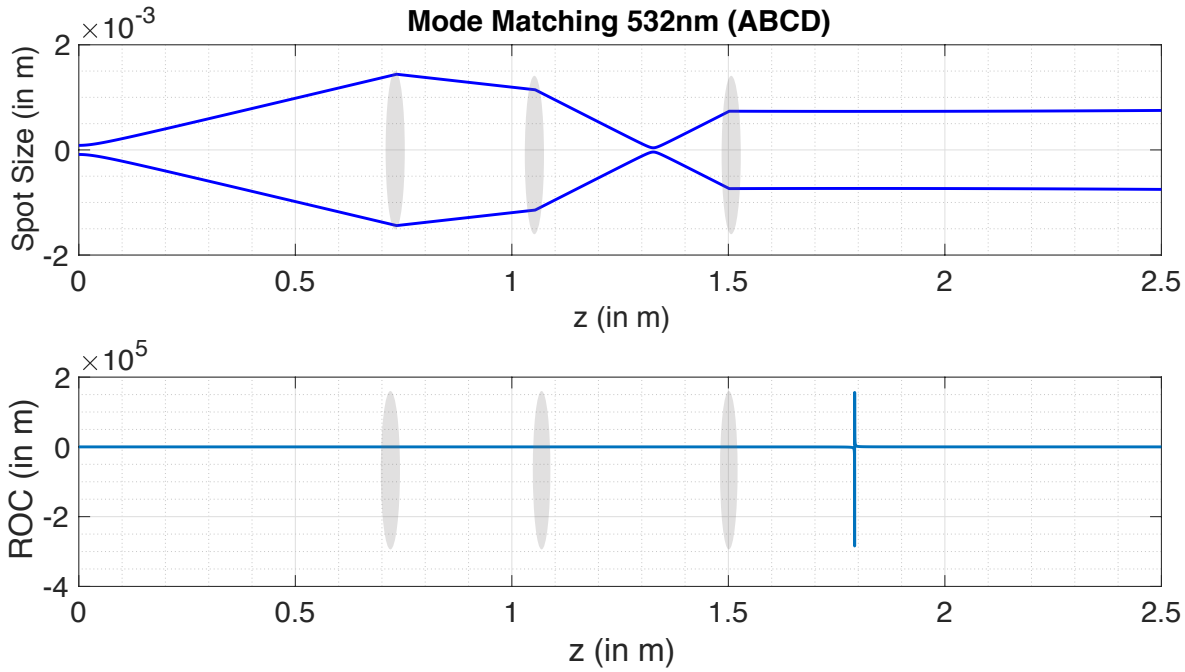

Figure 15: Mode Matching Solution for 532nm. (Waist at z=0)

The 3 lens solution Figure 15 is as follows -
f = 50cm at z = 73.4cm
f = 35cm at z = 105.4cm
f = 20cm at z = 150.2cm

According to this solution, the final beam waist is 720.4 μm which theoretically gives a coupling efficiency of 99.8%. The obtained coupling will be lower than this due to earlier mentioned reasons. The beam waist and location have been modified from the values obtained from the initial profiling by profiling the beam after the first two lenses.

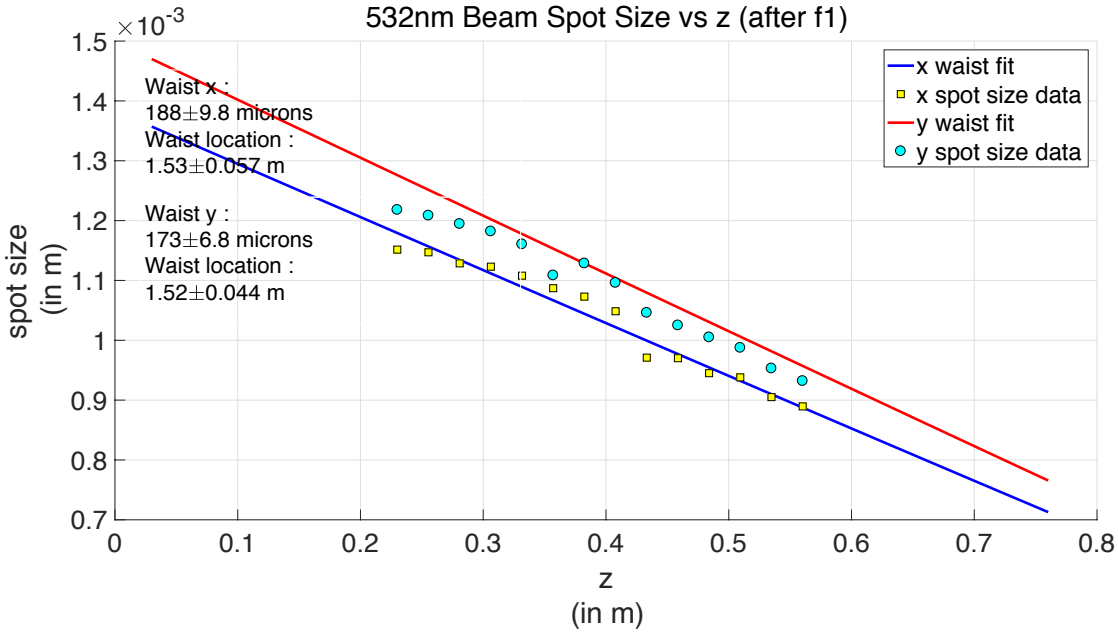

Figure 16: A 532nm beam profile after the first lens. z=0 is the location of the lens

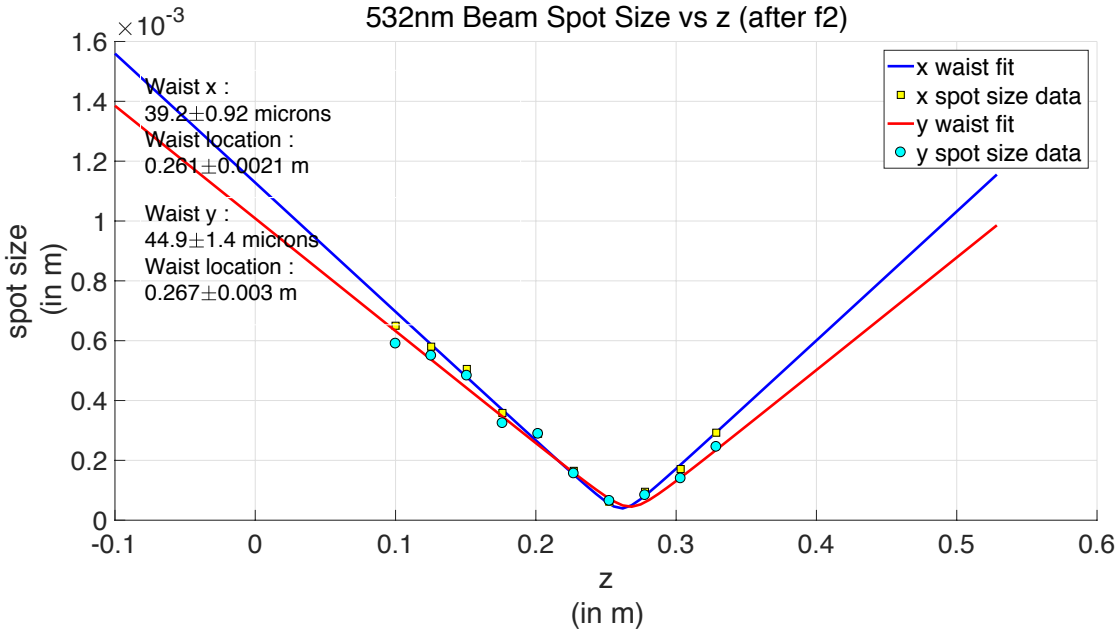

Figure 17: A 532nm beam profile after the second lens. z=0 is the location of the lens

Using the above configuration with some fine tuning, we managed to achieve around **77%** efficiency in coupling.

4.2 Squeezer Setup

The squeezer setup is shown in Figure 18. PD1 and PD2 are the photo-detectors for the homodyne detection measurement. The Dichroic mirrors are to remove any excess 532nm

light that is not attenuated by the single mode fibres.

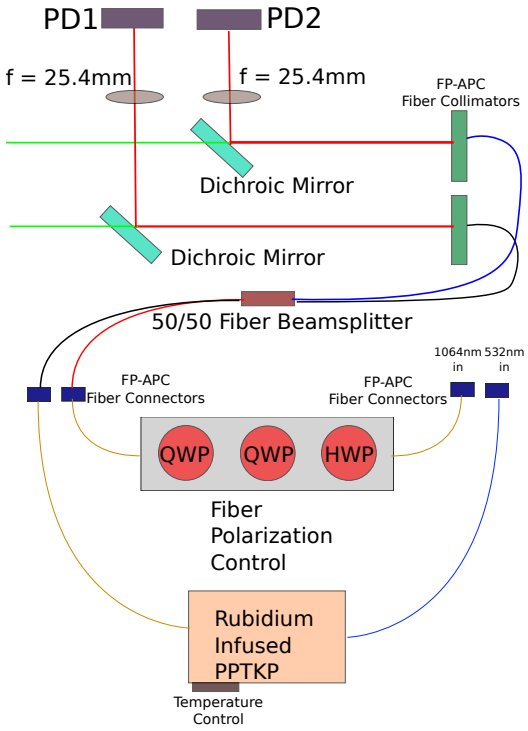

Figure 18: Waveguide Squeezer Setup

4.2.1 Characterisation of Waveguide

The non-linear waveguide is set up along with temperature control. Using the light coupled into the 1064nm fibre, we plotted phase matching curves for SHG (Second Harmonic Generation) the waveguide by varying its temperature and measuring 532nm output power. The obtained data was fit to a Sinc function [12]

$$I(\Delta kL) = I_{max}(\frac{sin(\Delta kL_c/2)}{\Delta kL_c/2})^2$$

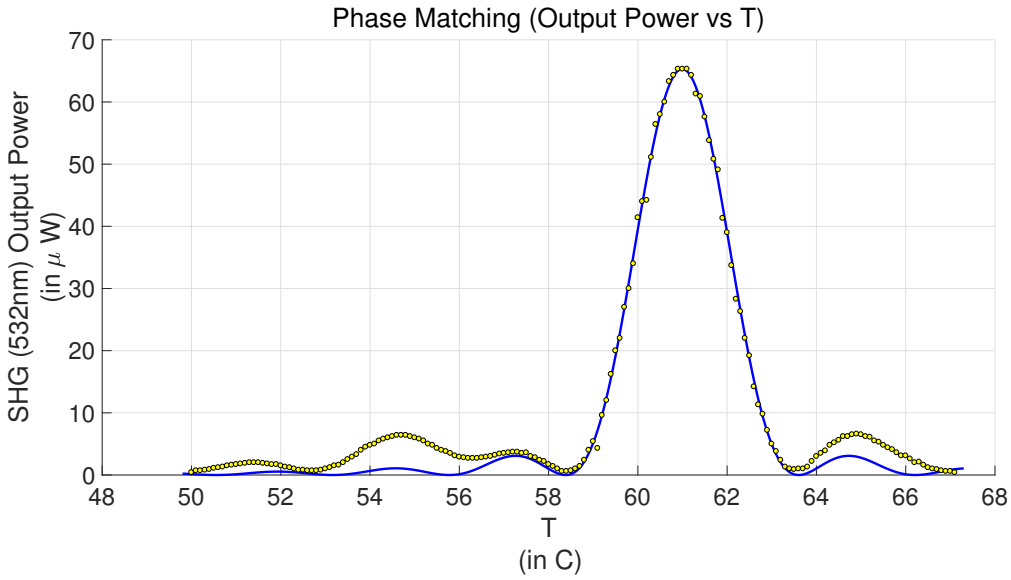

Figure 19: Phase Matching Calculations for input 1064nm power of 19.3mW

For 19.3mW of 1064nm input, we see that the peak SHG power acheived is 65.3μW at a temperature of 60.99°C. The curve has an FWHM width of 2.32°C. The lopsidedness of the data could be due to imperfections in the periodic polling of KTP. Assuming 50% loss at the end of the waveguide (as specified by the manufacturer), we find that the maximum conversion efficiency from 532nm to 1064nm (and the reverse process) is 1.353%.

4.2.2 Waveguide Mode Shape

The Rubidium Infused PPKTP waveguide is a 7 μm x 7 μm square waveguide. As described in Section 2.2.2, the solution is a separable in x and y. To solve for the exact values of μ_1 and μ_2, we must solve the following transcendental equation.

$$\mu \tan \mu = \sqrt{V^2 - \mu^2}$$

As the waveguide is symmetric, $\mu_1 = \mu_2 = \mu$ and $V_1 = V_2 = V$.

The value numerically obtained for μ is 0.8325. The mode shape obtained is shown in Figure 20

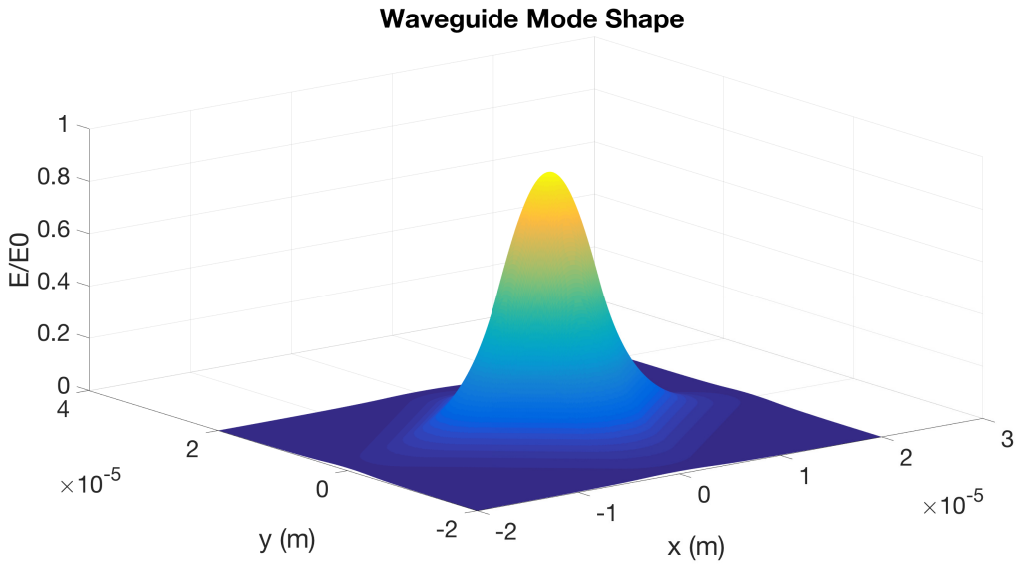

Figure 20: Waveguide Mode Shape

4.3 Homodyne Setup

The Homodyne Detection setup is shown in Figure 21. The photo-detectors are transimpedance amplifier circuits with 87% quantum efficiency InGaAs photodiodes(3mm diameter). We use the SR560 Pre-amp as the subtractor circuit in the homodyne detection and use a high-pass filter to eliminate the DC Offset of the signal. We then analyse the signal in frequency domain using the SR785 FFT Spectrum Analyser. The second photodetector circuit has variable gain so we can compensate for the beam-splitter imperfections in order to do a balanced homodyne detection.

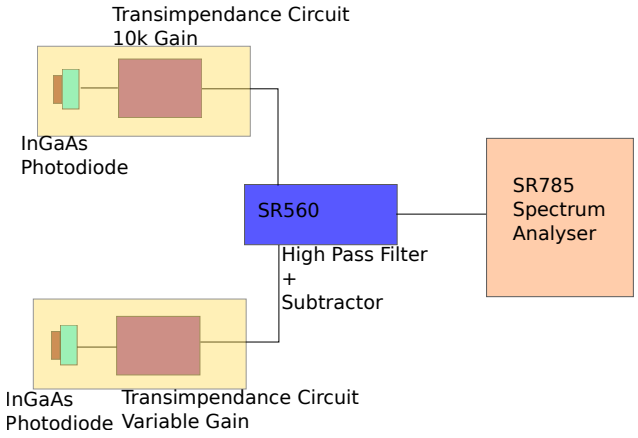

Figure 21: Block diagram of Homodyne Setup

For 1mW of light, we can assume that the photocurrent will be about 1mA. The shot noise corressponding to this would be $\sqrt{2eI}$ which is around $14.7\text{pA}/\sqrt{Hz}$. After a 10k gain this

would correspond to a voltage noise of $147\text{nV}/\sqrt{Hz}$

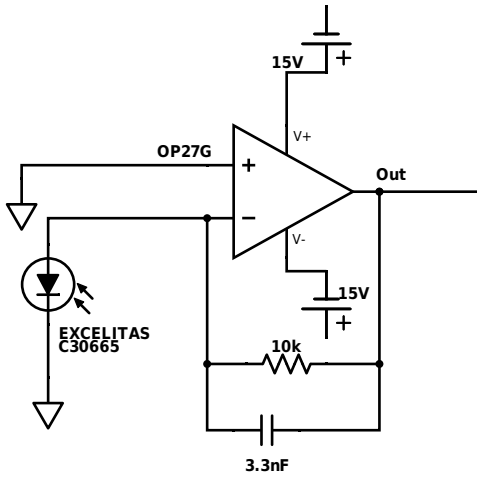

Figure 22: 10k Gain Photodetector

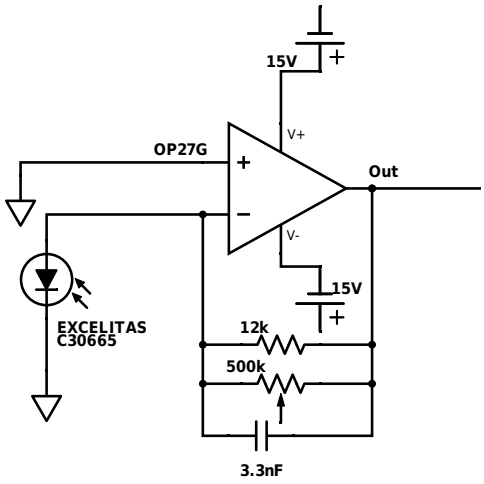

Figure 23: Variable Gain Photodetector

4.3.1 Noise Analysis of Photodetector Circuits

The schematics for the two photodetectors are given in Figures 22 and 23. The variable gain amplifier has gain ranging from 0 to 12K. The use of a capacitor across the transimpedance resistor is to balance the ringing caused by the internal capacitance of the photodiode. The dark noise plots of the circuits is given in the following plots. We find that the noise floor has about 10dB of clearance from the expected shot noise over most of the bandwidth.

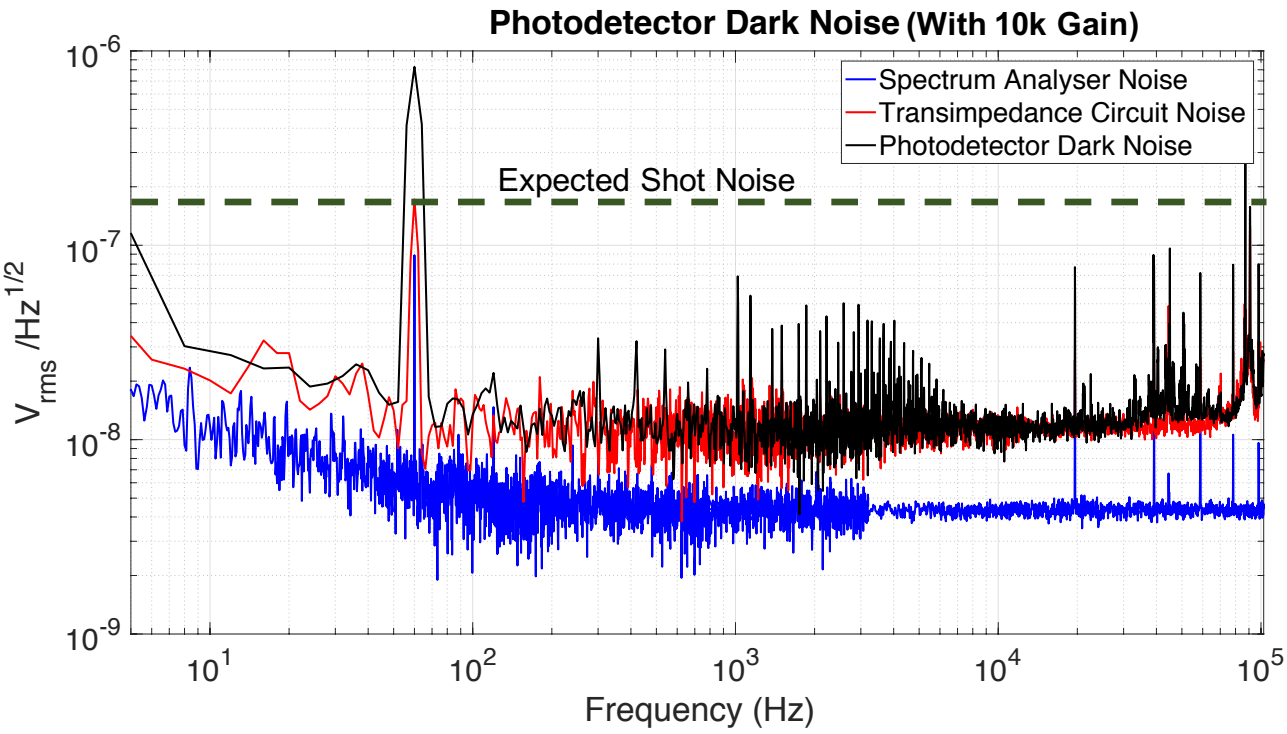

Figure 24: Photodetector Dark Noise(10K)

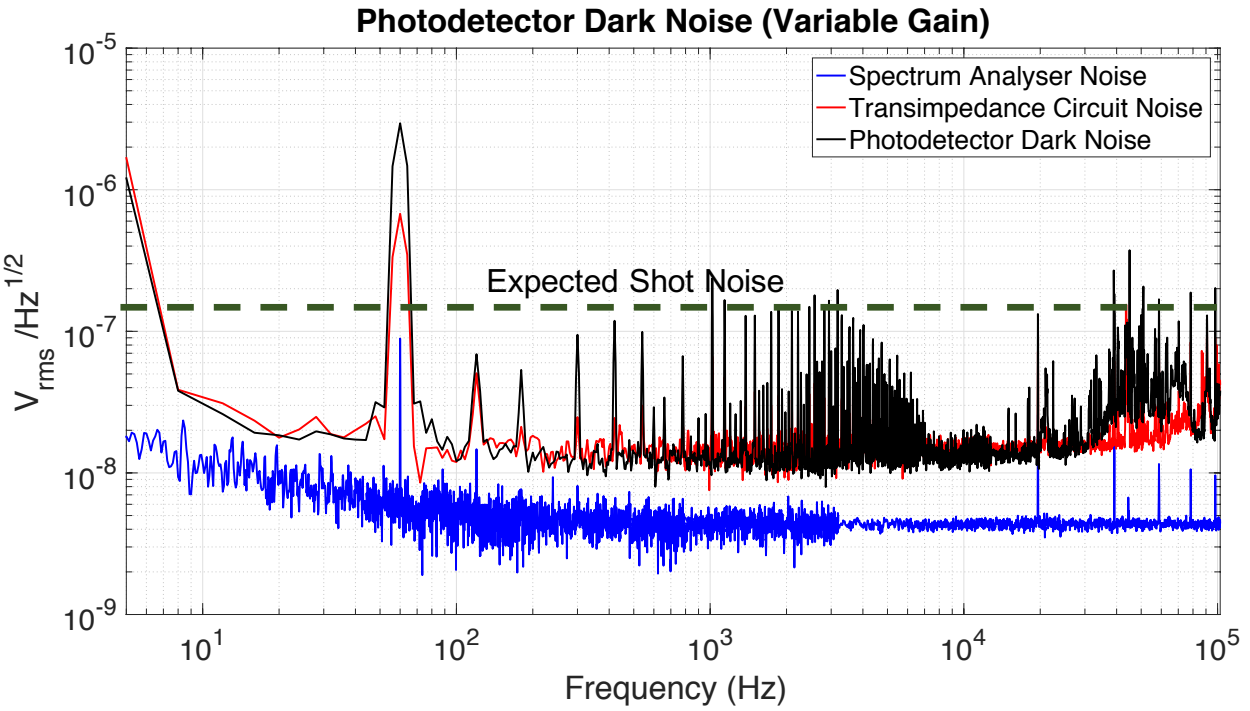

Figure 25: Photodetector Dark Noise(Variable)

4.4 Squeezing Losses

The following is a table with all the squeezing losses listed out.

Squeezing Losses	
Component	**Loss**
Waveguide	$\tilde{5}0\%$
Quantum Efficiency of Photodiode	$\tilde{1}3\%$
Beam Splitter (3% Error)	$\tilde{6}\%$
FP-APC Connectors	$\tilde{2}\%$
Total	$\mathbf{\tilde{6}0\%}$

Using the formula

$$V_{a'}^{out} = \eta_{loss} V_a^{in} + (1 - \eta)$$

,

we can calculate that the maximum obtainable squeezing at the detector is 3.3dB and for 3dB squeezing at the waveguide, we would measure around 1dB at the detector.

4.4.1 Mitigation of Waveguide loss

The waveguide, which has been butt-coupled to the single mode fibre, is the largest contributor to loss. It can be done in the following ways.

- Use a series of objectives after propagating this mode in free space. We can simulate the propagation and calculate the overlap using the FFT code described in the beginning of the report.
- Use a custom waveguide design in order to maximize the overlap between the waveguide mode and fibre modes.

5 Acknowledgments

I would like to thank LIGO, Caltech, NSF and IndIGO for giving me an opportunity to SURF with LIGO at W. Bridge. I would like to thank my mentor, Andrew Wade, for helping me with literally everything during my 11 week stay. I would also like to thank Eric Gustafson and Hiro Yamamoto for their invaluable insight into the world of optics, and Koji Arai for patiently helping me with the electronics of the homodyne detector . I would like to thank Rana Adhikari for teaching me how to make pretty plots and do comprehensive error analysis and also for getting me very interested in experimental physics. I would also like to thank the Kavli foundation who, according to Rana, made all of this possible.

I would finally like to thank Dr. Joyee Ghosh at IIT Delhi for introducing me to the concept of squeezed light and encouraging me to apply for this program.

6 Appendix

6.1 Beam Profiling

The properties of the Gaussian beam depend only on the size of the waist w_0 and the wavelength λ. It is therefore possible to fully characterize a Gaussian beam by determining the size and location of the beam waist. To determine these quantities, we make a series of 'knife edge' measurements to determine the spot size on different axial locations.

We record the total power in the beam as a knife edge is translated through the beam using a calibrated translation stage. This gives us the integral of the power from $-\infty$ to the knife edge location.

In one direction this power is given by

$$P(y) = \frac{P_{total}}{2}(1 - \mathrm{erf}(\frac{\sqrt{2}(y - y_0)}{w_y}))$$

Fitting the obtained power to the above function gives us the spot size at the location of profiling

The obtained spot sizes are fit to the function

$$w(z) = w_0\sqrt{1 + (\frac{z - z_0}{z_r})^2}$$

where $z_r = \dfrac{\pi w_0^2}{\lambda}$

in order to find the beam waist size and location.

References

[1] LIGO Scientific Collaboration, *Advanced LIGO*. Class. Quant. Gravity 32, 074001 (2015)

[2] Buonanno, Alessandra and Chen, Yanbei, *Quantum noise in second generation, signal-recycled laser interferometric gravitational-wave detectors*

PhysRevD.64.042006

[3] LIGO Scientific Collaboration, *Instrument Science White Paper*. LIGO-T1600119v4 https://dcc.ligo.org/LIGO-T1600119/public

[4] LIGO Scientific Collaboration, *Enhanced sensitivity of the LIGO gravitational wave detector by using squeezed states of light* Nature Photonics 7, 613619 (2013)

[5] LIGO Scientific Collaboration, *A gravitational wave observatory operating beyond the quantum shot-noise limit* Nature Phys. 7, 962965 (2011)

[6] Alex Lvovsky, *Squeezed Light*. arXiv:1401.4118 .

[7] Keisuke Goda et al, *A Quantum-Enhanced Prototype Gravitational-Wave Detector*. In: 4.June (2008), p. 7. doi: 10.1038/nphys920. arXiv: 0802.4118

[8] A. Ghatak and K. Thyagrajan , *Chapter 14, Optical Electronics*.

[9] Anthony Siegman, *Chapter 20, Lasers*.

[10] The Virgo Collaboration *Chapter 3, The VIRGO Physics Book Vol II - Optics and Related Topics*.

[11] M.S. Stefszky et al, *Balanced Homodyne Detection of Optical Quantum States at Audio-Band Frequencies and Below*.

[12] Sheia Dwyer *Quantum noise reduction using squeezed states in LIGO(Thesis)*

[13] Hiro Yamamoto *Separation of adaptive scaling in the field propagation in x and y* LIGO-T1300995-v1